Hindawi
Shock and Vibration
Volume 2020, Article ID 8888065, 11 pages
https://doi.org/10.1155/2020/8888065

*Research Article*

# Safety Characteristic Evaluation of Cage in Cylindrical Roller Bearing at the Stage of Start-Up and Stop

**Zhang Wenhu,[1,2] Wu Zhimin,[3] Deng Sier,[1] Zhang Song,[2] Tian Heng,[1] and Yang Haisheng[1]**

[1]*School of Mechatronics Engineering, Henan University of Science and Technology, Luoyang 471003, China*
[2]*Post-Doctoral Research Center of Changzhou NRB Corporation, Changzhou 213001, China*
[3]*School of Mechanical and Electrical Engineering, Shenzhen Polytechnic, Shenzhen 518055, China*

Correspondence should be addressed to Wu Zhimin; zhimin_wu@szpt.edu.cn

Received 21 May 2020; Revised 16 July 2020; Accepted 25 August 2020; Published 4 September 2020

Academic Editor: Dr Mahdi Mohammadpour



The dynamics model of cylindrical roller bearing (CRB) in aeroengine main shaft was promoted and solved by Hilber–Hughes–Taylor (HHT) integer algorithm with variable step in combination with symmetric multiprocessing (SMP) parallel solving technology, and a finite element model of roller to cage contact was built. The dynamic characteristics of CRB at the stage of start-up and stop were analyzed firstly, and then, the collision forces between rollers and cage were used as the boundary conditions of the finite element model to discuss the influences of working conditions, structural parameters, and materials on the stress distribution and safety characteristic of cage at the stage of start-up and stop. The findings will provide the theoretical basis for the designing of CRB in aeroengine main shaft.

## 1. Introduction

The failures of CRB in aeroengine main shaft happen more frequently at the stage of start-up and stop, due to a sudden change in rotating speed and load. At the stage of start-up and stop, a greater acceleration of CRB causes a sudden increase or decrease in the rotating speed of cage and rollers, which arouses a chain reaction in the changes of collision forces and collision frequencies between cage and rollers. The frequent collisions between cage and rollers accelerate the failure of cage and thereby affect the normal operation of machine.

Gupta [1–3] firstly developed a dynamics model of CRB with six degrees of freedom and focused on the effect of cage's pocket clearance, guide clearance on its whirl orbit, and slip ratio. Ghaisas, Wassgren, and Sadeghi [4] developed a six-degree-of-freedom dynamics model of CRB to simulate cage's instability under the conditions of light load and high speed. They studied the effect of cage pocket clearance, cage asymmetry, roller diameter, and tilting angle of inner ring and various roller crown profiles on cage's dynamic behaviors. Jafar and Khonsaria [5] hold the view that the lubricant's traction characteristic has a big impact on cage's behaviors in CRB and then analyzed cage's rotational speed under a simplified traction model and MIL-L-7808 traction model. Cui [6] built a quasi-dynamic model of CRB and then studied cage's dynamic behaviors. Yang and Deng [7] developed a rigid-flexible dynamics model of CRB, based on the modified Craig–Bampton substructure modal synthesis method and compared the dynamic behaviors of flexible cage with that of rigid cage. Liu et al. [8] analyzed the impact of working conditions and structure parameters on cage's stability. Deng and Deng et al. [9] built a dynamics model of the intermediate CRB in aeroengine main shaft and analyzed cage's guidance method, ratio of pocket clearance, and working conditions on cage's stability. Chen et al. [10] applied the chaos theory to investigate the influence of cage's guidance gap and eccentricity on its dynamic behaviors in CRB. Fang et al. [11] developed a finite element model of cage in typical CRB to study the stress concentration factors, but the actual forces acting on the cage

when bearing is working were not involved. Dib and Haiahem [12] did a FEM analysis of cage's stress distribution in CRB and pointed out that the traction stress is the cause of cage's failure and the stress distribution is located in the edge of cage's pocket. Yang et al. [13] presented a dynamics model of high-speed CRB with the flexible cage and pointed out that cage is easy to bear a higher alternating stress at the intersectional point of bar and side bar, at which cage has a hazard of suffering from a fatigue fracture. Li [14] built a dynamics model of CRB and then focused on the influence of working conditions and structural parameters on cage's slip ratio at the stop stage. Jia and Deng [15] built a nonlinear dynamics model of high-speed CRB and studied the effect of radial loads, accelerations of inner ring, viscosity of lubricating oil, and structural parameters on the slip characteristic at the start-up stage. Ding et al. [16] built a nonlinear dynamics model of high-speed CRB, and then the effects of acceleration, radial load and radial clearance on cage's speed, and slip characteristic were investigated. Cui et al. [17–20] presented a nonlinear dynamics model of CRB with the dynamic unbalance of roller and cage and then focused on the impact of roller's dynamic unbalance on cage's stability, stress distribution, and vibration. Niu et al. [21] presented a nonlinear dynamics model of CRB to predict roller's skidding behavior, considering the radial clearance, roller crown profile, and discontinuous contact between roller and cage and investigated the influence of various load conditions on single roller's local skids. Sun et al. [22] presented a dynamics model of CRB with the elastic ring support and then investigated the influences of structural parameters of elastic ring support and working conditions on the vibration characteristic. Deng et al. [23] presented a nonlinear dynamics model of CRB with a trilobe-raceway and investigated the influences of structural parameters and the tolerance of the trilobe-raceway, working conditions and outer ring's installation method on cage's slip characteristic. All the above-mentioned researches mainly focused on the influence of bearing working conditions, structural parameters, and cage's guidance on cage's dynamic behavior and stability when CRB is working at a constant speed or various loads. Only few studies had involved cage's dynamic characteristics or behaviors at the stage of start-up and stop. However, the study about cage's stress distribution and safety characteristic has not aroused the adequate attentions, especially for CRB withstanding frequent start-up and stop.

In this paper, a dynamics model of CRB at the stage of start-up and stop and a finite element model of roller to cage contact are developed. The dynamic characteristics, stress distribution, and safety characteristic of cage are investigated. The findings provide a theoretical basis for the designing of CRB's cage in aeroengine main shaft.

## 2. Computational Model of the Frictional Coefficient

For CRB at the stage of start-up and stop, the lubrication states between rollers and raceways change from time to time and can be categorized into three types: boundary lubrication, mixing lubrication and EHL (elastohydrodynamic lubrication), corresponding to the different frictional coefficients. In order to build a precise dynamics model of CRB, the frictional coefficient between two contact surfaces lubricated by aviation lubricant oil 4109 must be measured by using the self-made test rig in [24]. However, in the test process, it is found that the lubrication states between the disc specimen and the ball specimen cannot be controlled precisely. Consequently, the test rig is powerless to measure the boundary frictional coefficient and mixing frictional coefficient, but the measurement results of frictional coefficients under EHL state are trustworthy, and then the formula of EHL frictional coefficient $\mu_{\mathrm{EHL}}$ is obtained by applying the curve fitting technic to the test data:

$$\mu_{\mathrm{EHL}} = (A + BS)e^{-CS} + D. \tag{1}$$

In (1), $A$, $B$, $C$, $D$ are the functions of normal load, lubrication temperature of inlet, and velocity of contact surface, respectively; $S$ is slide-roll ratio. The detailed expressions of $A$, $B$, $C$, and $D$ for 4109 are shown in [24].

For the frictional coefficients under the boundary lubrication state and the mixing lubrication state, according to [25], the frictional coefficient $\mu$ under various lubrication states can be expressed as

$$\mu = \begin{cases} \mu_{\mathrm{BL}}, & (-0.1 + 22.28S)e^{-181.46S} + 0.1, \\ \mu_{\mathrm{ML}}, & \dfrac{\mu_{BL} - \mu_{EHL}}{(0.06 - 3.0)^6}(\lambda - 3.0)^6 + \mu_{\mathrm{EHL}}, \\ \mu_{\mathrm{EHL}}, & (A + BS)e^{-CS} + D. \end{cases} \tag{2}$$

In (2), $\lambda$ is the lubricant film parameter, $\lambda = (h_{\min}/\sqrt{\sigma_1^2 + \sigma_2^2})$, $h_{\min}$ is minimum film thickness, and $\sigma_1$ and $\sigma_2$ are the root mean square (RMS) roughness of two contact bodies; $\mu_{\mathrm{BL}}$ is the frictional coefficient under boundary lubrication state, $\lambda < 0.06$; $\mu_{\mathrm{ML}}$ is the frictional coefficient under mixing lubrication state, $0.06 \le \lambda < 3.0$; $\mu_{\mathrm{EHL}}$ is the frictional coefficient under EHL state, $\lambda \ge 3.0$.

## 3. Dynamics Model of CRB at the Stage of Start-Up and Stop

In this paper, CRB only bears a radial force $F_r$, outer ring is fixed, inner ring rotates, cage is guided by outer ring, the mass center of each bearing component coincides with its centroid, and bearing is lubricated by aviation lubricant oil 4109.

In order to describe the interaction forces and movement relationships of components in CRB, the following five coordinate systems are defined in Figure 1 (refer to [26]).

*3.1. Nonlinear Dynamics Differential Equations of Roller.* When CRB is working, rollers are simultaneously acted by inner raceway, outer raceway, and cage, as shown in Figure 2.

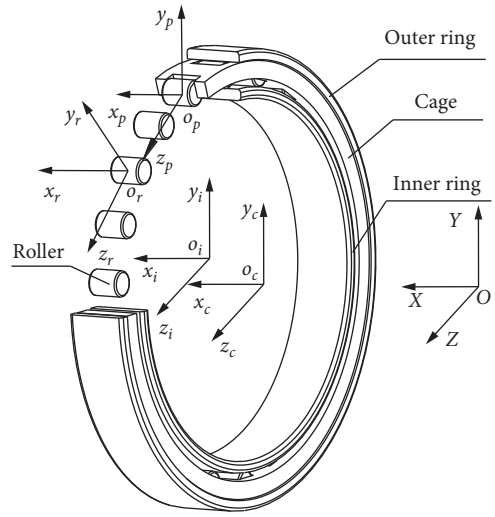


Figure 1: Coordinate systems of CRB.

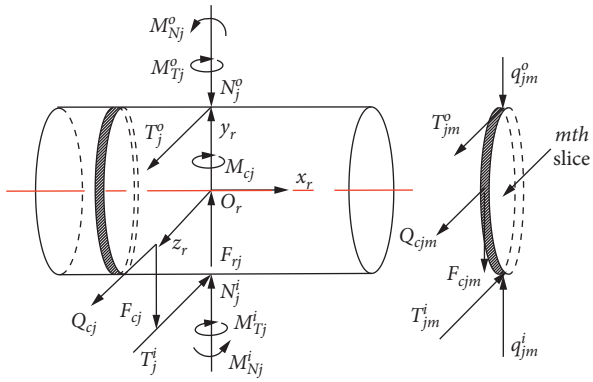


Figure 2: Schematic diagram of roller forces.

Subscript {i, o} represent inner raceway and outer raceway, respectively; $N^i_j$, $N^o_j$ are the normal force between the $j$th roller and raceways; $T^i_j$, $T^o_j$ are the oil drag force between the $j$th roller and raceways; $M^i_{Nj}$, $M^o_{Nj}$ are the additional moment due to $N^i_j$ and $N^o_j$; $M^i_{Tj}$, $M^o_{Tj}$ are the additional moment due to $T^i_j$ and $T^o_j$; $Q_{cj}$, $F_{cj}$ are the normal force and tangential friction force between the $j$th roller and cage's cross beam; $M_{cj}$ is the additional moment due to $F_{cj}$; $F_{rj}$ is the centrifugal force of the $j$th roller; $q^i_{jm}$, $q^o_{jm}$ are the collision forces between the $m$th slice and raceways; $T^i_{jm}$, $T^o_{jm}$ are the oil drag forces between the $m$th slice and raceways; $Q_{cjm}$, $F_{cjm}$ are the normal force and tangential friction force between the $m$th slice and cage's cross beam. The detailed expresses of symbols in Figure 2 refer to [26].

Nonlinear dynamics differential equations of the $j$th roller are shown as follows:

$$\begin{cases} m_r y_{rj} = -N^i_j \cos\varphi_j + N^o_j \cos\varphi_j - Q_{cj} \sin\varphi_j - F_{mj} \cos\varphi_j - T^i_j \sin\varphi_j + T^o_j \sin\varphi_j - F_{cj} \cos\varphi_j, \\ m_r z_{rj} = N^i_j \sin\varphi_j - N^o_j \sin\varphi_j - Q_{cj} \cos\varphi_j + F_{mj} \sin\varphi_j - T^i_j \cos\varphi_j + T^o_j \cos\varphi_j + F_{cj} \sin\varphi_j, \\ J_{rx} \dot{\omega}_{rjx} = -T^i_j \dfrac{D_w}{2} - T^o_j \dfrac{D_w}{2} + F_{cj} \dfrac{D_w}{2}, \\ J_{ry} \dot{\omega}_{rjy} = -M^i_{Tj} \sin\varphi_j - M^o_{Tj} \sin\varphi_j + M_{cj} \cos\varphi_j + M^i_{Nj} \sin\varphi_j + M^o_{Nj} \sin\varphi_j, \\ J_{rz} \dot{\omega}_{rjz} = -M^i_{Tj} \cos\varphi_j - M^o_{Tj} \cos\varphi_j - M_{cj} \sin\varphi_j + M^i_{Nj} \cos\varphi_j + M^o_{Nj} \cos\varphi_j. \end{cases} \tag{3}$$

In (3), $m_r$ is roller mass; $\varphi_j$ is the azimuth angle of the $j$th roller; $D_w$ is roller diameter; $\ddot{y}_{rj}$, $\ddot{z}_{rj}$ are displacement accelerations of the $j$th roller's mass center in {$O$; $X$, $Y$, $Z$}; $J_{rx}$, $J_{ry}$, $J_{rz}$ are moments of inertia of roller in {$O$; $X$, $Y$, $Z$}, respectively; $\dot{\omega}_{rjx}$, $\dot{\omega}_{rjy}$, $\dot{\omega}_{rjz}$ are angular accelerations of the $j$th roller in{$O$; $X$, $Y$, $Z$}.

*3.2. Nonlinear Dynamics Differential Equations of Cage.* When CRB is working, cage is simultaneously acted by collision force of rollers, guiding force of outer ring and combined resistance of oil/air mixture to cage's surfaces. The forces acting on cage are shown in Figure 3.

In Figure 3, $\{o; y, z\}$ is reference coordinate system of cage; $e_c$ is offset of cage center; $\Delta_{yc}$, $\Delta_{zc}$ are components of $e_c$ along $y$-axis and $z$-axis, respectively; $\Psi_c$ is angle between $\{o_c; y_c, z_c\}$ and $\{o; y, z\}$; $F'_{cy}$, $F'_{cz}$, $M'_{cx}$ are forces and moment caused by hydrodynamic action between cage centering surface and outer ring guiding surface, respectively; $T_{\mathrm{CDS}}$ and $T_{\mathrm{CDO}}$ are resistances of cage end-surface and cage surface caused by oil/air mixture, respectively. The expressions of $F'_{cy}$, $F'_{cz}$, $M'_{cx}$, $T_{\mathrm{CDS}}$, and $T_{\mathrm{CDO}}$ refer to [27].

Nonlinear dynamics differential equations of cage are shown as follows:

$$\begin{cases} m_c y_c = \sum_{j=1}^{RN}\left(Q_{cj}\sin\varphi_j + F_{cj}\cos\varphi_j\right) + F'_{cy}\cos\psi_c + F'_{cz}\sin\psi_c - G_c, \\ m_c z_c = \sum_{j=1}^{RN}\left(Q_{cj}\cos\varphi_j - F_{cj}\sin\varphi_j\right) + F'_{cy}\sin\psi_c - F'_{cz}\cos\psi_c, \\ J_{cx}\dot{\omega}_{cx} = \sum_{j=1}^{RN}\left(F_{cj}\frac{D_w}{2}\right) - M'_{cx} - T_{\mathrm{CDO}} - T_{\mathrm{CDS}}, \\ J_{cy}\dot{\omega}_{cy} = \sum_{j=1}^{RN}\left(-M_{cj}\cos\varphi_j\right), \\ J_{cz}\dot{\omega}_{cz} = \sum_{j=1}^{RN}\left(M_{cj}\sin\varphi_j\right). \end{cases} \tag{4}$$

In (4), $m_c$ is cage mass; $G_c$ is cage gravity; $\ddot{y}_c$, $\ddot{z}_c$ are displacement accelerations of cage's mass center in $\{O; X, Y, Z\}$; $J_{cx}$, $J_{cy}$, $J_{cz}$ are moments of inertia of cage in $\{O; X, Y, Z\}$; $\dot{\omega}_{cx}$, $\dot{\omega}_{cy}$, $\dot{\omega}_{cz}$ are angular accelerations of cage in $\{O; X, Y, Z\}$; $RN$ is the number of rollers.

*3.3. Nonlinear Dynamics Differential Equations of Inner Ring.* Nonlinear dynamics differential equations of inner ring are shown as follows:

$$\begin{cases} m_i y_i = \sum_{j=1}^{RN}\left(N_j^i\cos\varphi_j + T_j^i\sin\varphi_j\right) - F_r, \\ m_i z_i = \sum_{j=1}^{RN}\left(-N_j^i\sin\varphi_j + T_j^i\cos\varphi_j\right), \\ J_{ix}\dot{\omega}_{ix} = \sum_{j=1}^{RN} T_j^i\frac{D_w}{2}, \\ J_{iy}\dot{\omega}_{iy} = \sum_{j=1}^{RN}\left(M_{Tj}^i\sin\varphi_j\right), \\ J_{iz}\dot{\omega}_{iz} = \sum_{j=1}^{RN}\left(M_{Tj}^i\cos\varphi_j\right). \end{cases} \tag{5}$$

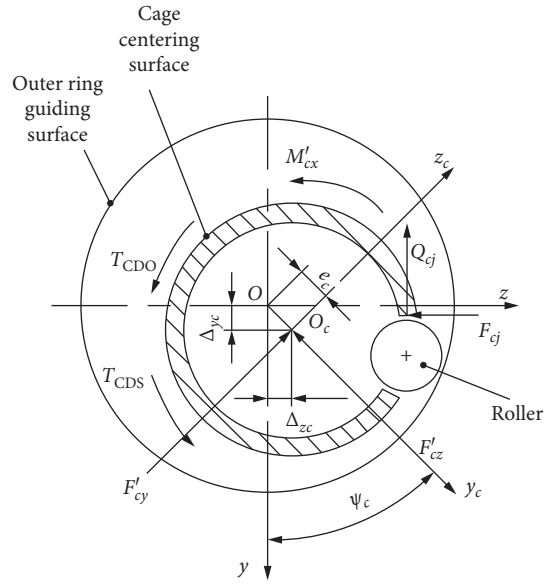


Figure 3: Schematic diagram of cage forces.

In (5), $m_i$ is mass of inner ring; $\ddot{y}_i$, $\ddot{z}_i$ are displacement accelerations of inner ring mass center in $\{O; X, Y, Z\}$; $J_{ix}$, $J_{iy}$, $J_{iz}$ are moments of inertia of inner ring in $\{O; X, Y, Z\}$; $\dot{\omega}_{ix}$, $\dot{\omega}_{iy}$, $\dot{\omega}_{iz}$ are angular accelerations of inner ring in $\{O; X, Y, Z\}$.

## 4. Dynamic Characteristics and Finite Element Model at the Stage of Start-Up and Stop

Nonlinear dynamics differential equations (3)–(5) were solved by Hilber–Hughes–Taylor (HHT) integer algorithm with variable step in combination with symmetric multiprocessing (SMP) parallel solving technology; refer to [26] and [28–30]. The material of ring and roller is 8Cr4Mo4V, and the material of cage is 40CrNiMo. The main parameters of CRB are shown in Table 1.

*4.1. Dynamic Characteristics of the Roller and Cage.* Change curves of speed of inner ring and cage with time at the stage of start-up are shown in Figure 4(a), and the detailed picture of Figure 4(a) is shown in Figure 4(b). Change curves of collision forces between all rollers and cage's cross beam with time at the stage of start-up are shown in Figure 5. The fluctuation of cage's speed is obvious at the beginning of acceleration (time < 0.045 s) when accelerating from 0 r/min to 10000 r/min, with the greater collision forces between rollers and cage's cross beam, and the more frequent collisions. And the collision forces with positive values indicate that rollers drive cage to accelerate at the stage of start-up. When acceleration time is longer than 0.045 s, the speed of cage increases nearly linearly, and collision forces between cage's cross beam and rollers are comparatively smaller. When CRB is working at constant speed (time-> 0.3 s), cage's speed shows almost no fluctuation.

Change curves of speed of inner ring and cage with time at the stage of stop are shown in Figure 6. Change curves of

Table.1: The main parameters of bearing.

| Item | Value |
|---|---|
| Bearing outside diameter (mm) | 122 |
| Bearing bore diameter (mm) | 82 |
| Bearing width (mm) | 19 |
| Number of rollers | 22 |
| Diameter of roller (mm) | 10 |
| Length of roller (mm) | 10 |
| Cage pocket circumferential clearance (mm) | 0.48 |
| Guide clearance of cage (mm) | 1.2 |
| Bearing radial clearance (mm) | 0.01 |
| Roughness of roller ($\mu$m) | 0.08 |
| Roughness of inner raceway ($\mu$m) | 0.1 |
| Roughness of outer raceway ($\mu$m) | 0.1 |
| Roughness of cage ($\mu$m) | 0.1 |

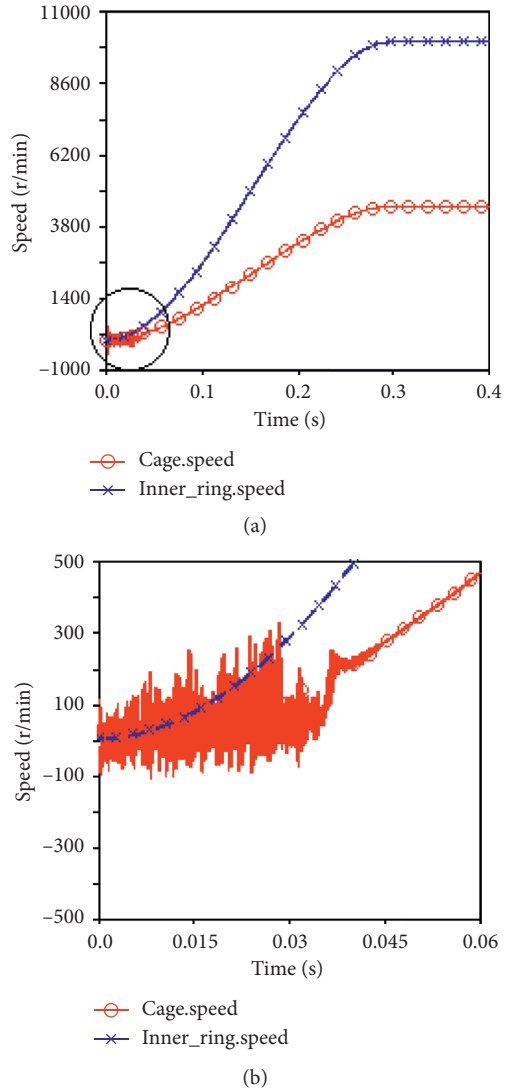


Figure 4: Speeds of inner ring and cage at the stage of start-up.

collision forces between all rollers and cage's cross beam with time at the stage of stop are shown in Figure 7.

As Figures 6 and 7 shows, cage's speed shows almost no fluctuation when CRB is working at constant speed

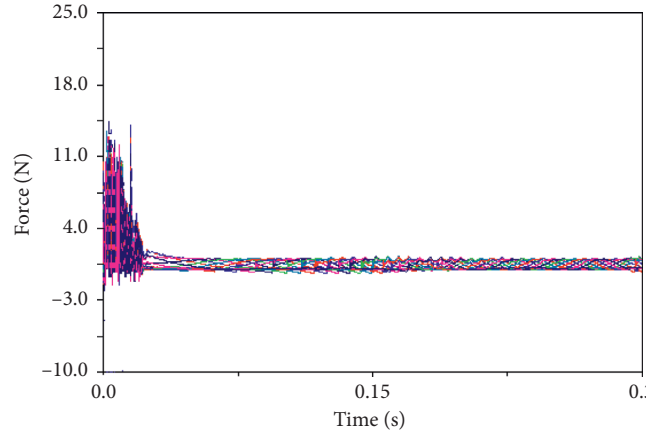


Figure 5: Collision forces between all rollers and cage's cross beam at the stage of start-up.

(time < 0.1 s). But in deceleration process (time > 0.1 s), cage's speed decreases nearly linear with time, and there is a speed difference between roller and cage, which leads to greater collision forces between cage's cross beam and rollers. And the collision forces with negative values indicate that rollers enforce cage to decelerate at the stage of stop.

*4.2. Finite Element Model of the Roller to Cage Contact.* The finite element model of roller to cage contact in Figure 8 was built in ANSYS, and the following assumptions were made:

(1) The collision force between cage and guiding ring was neglected

(2) Roller's skewing and tilting were neglected, because that the skewing angle and tilting angle were very small at the stage of start-up and stop

(3) The friction between roller and cage was neglected

In Figure 9, the roller and cage were meshed with the SOLIID 186 element, and the contact 174 element and target 170 element were used to define the contact regions of roller and cage's cross beam, respectively. The element size of cage and contact region of roller was 0.5 mm and the element size of noncontact region of roller was 2 mm.

Under different working conditions, the count of loaded rollers is different, and then the number of rollers with the largest collision force at the start-up and stop stage is also variable. It may be the first roller or the $j$th roller. Therefore, according to the results of collision forces under different working conditions, such as Figures 5 and 7, roller with the largest collision force was chosen as the object of finite element model. The detailed boundary conditions were as follows:

(1) The radial displacement of roller was constrained in the cylindrical coordinate system.

(2) The collision force $Q_{cj}$ calculated by dynamic method acted on the center plane of roller in Figure 8. And we must point out that we only choose the moment

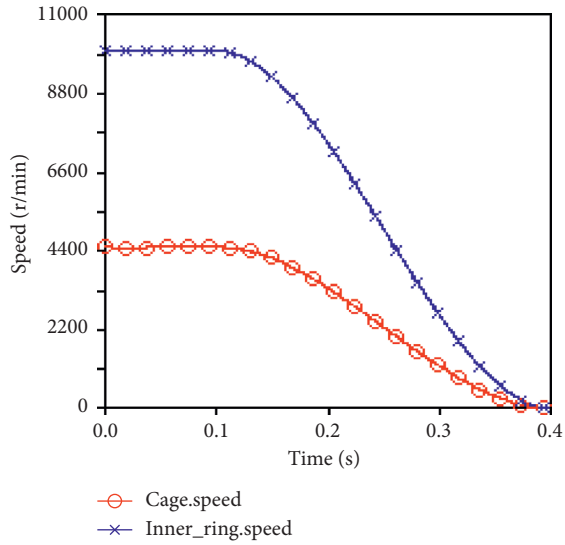


Figure 6: Speed of inner ring and cage at the stage of stop.

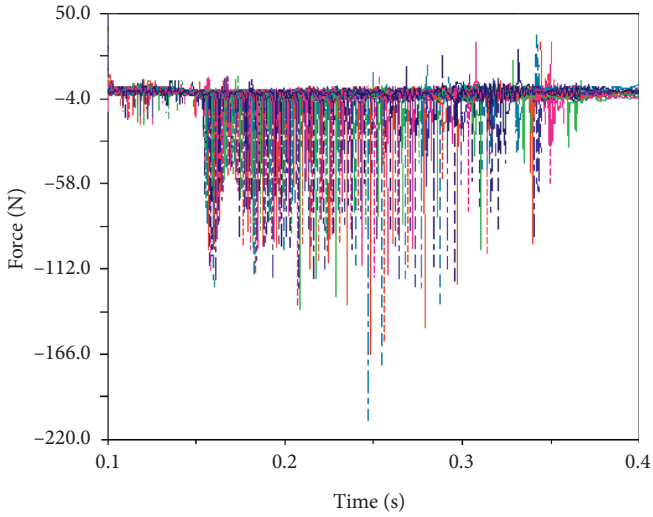


Figure 7: Collision forces between all rollers and cage at the stage of stop.

with relatively large collision forces as the boundary condition in order to improve the computational efficiency.

(3) The angular speeds of roller and cage acted on roller and cage, respectively.

## 5. Analysis of Cage Stress and Safety Characteristic at the Stage of Start-Up and Stop

Fatigue failure of cage always emerges at the connection of crossbeam and side beam, which coincides with the same findings in [13]. Therefore, this study focuses on von Mises stress at the connection of crossbeam and side beam. The safety factor Fs of fatigue failure is used to evaluate the safety

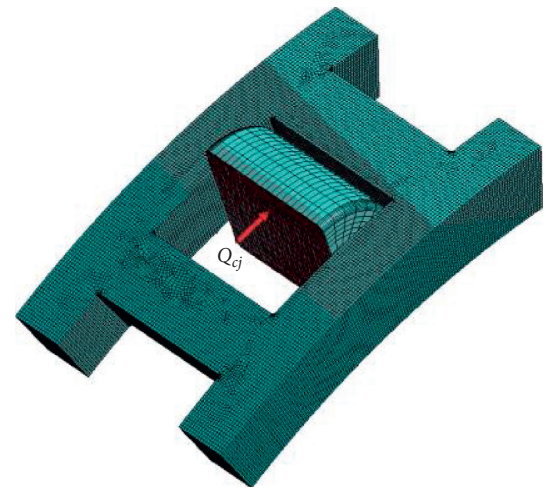


Figure 8: Finite element model of roller to cage contact.

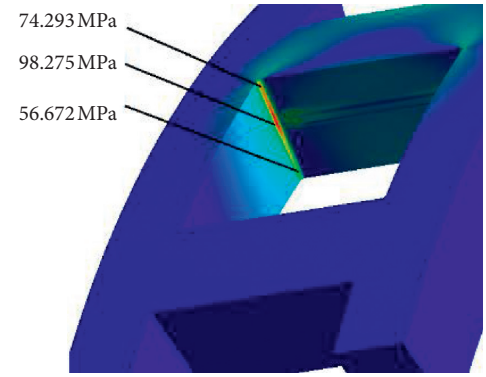


Figure 9: von Mises stress of the connection of crossbeam and side beam at the stage of stop.

characteristic of cage and is expressed as follows in [31] and [32]:

$$F_s = \frac{S_{\text{limit}}}{\sigma_e}, \tag{6}$$

where $S_{\text{limit}}$ is ultimate tensile strength of material and $\sigma_e$ is maximum von Mises stress.

*5.1. Analysis of Cage Stress Distribution.* Through the preliminary analysis of Section 3, it is shown that cage stress at the stage of start-up is mainly aroused by collision forces between rollers and cage. But at the stage of stop, cage stress is aroused by high speed of cage and collision forces between rollers and cage together. Stress distributions of cage at the stage of start-up and stop are shown in Figures 9 and 10, respectively.

In Figures 9 and 10, at the stage of start-up, the maximum von Mises stress at the connection of crossbeam and side beam appears in the middle of connection. However, at the stage of stop, the maximum von Mises stress at the connection of crossbeam and side beam is close to cage's

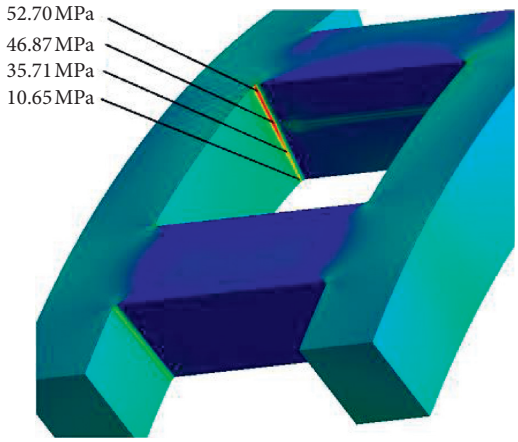


Figure 10: von Mises stress of the connection of crossbeam and side beam at the stage of start-up.

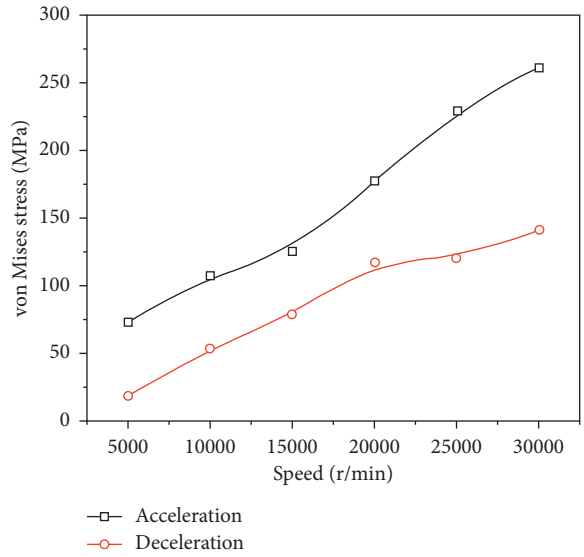


Figure 11: Influence of inner acceleration on cage stress at the stage of start-up and stop.

external surface, due to the high speed of cage. And the higher the speed of cage is, the closer the maximum von Mises stress is to cage's external surface.

*5.2. Influence of Inner Ring Acceleration on Cage Safety Characteristic.* Assuming that radial force is set to 1000 N, speeds of inner ring are set to 5000 r/min, 10000 r/min, 15000 r/min, 20000 r/min, 25000 r/min, and 30000 r/min, respectively. Acceleration time and deceleration time are set to 0.3 s. Changing trends of maximum von Mises stress with acceleration at the connection of crossbeam and side beam are shown in Figure 11. The maximum von Mises stress increases with the acceleration of inner ring at the stage of start-up and stop. And the maximum von Mises stress at the stage of start-up is generally greater than that at the stage of stop.

According to [33], the ultimate tensile strength of 40CrNiMo is 980 MPa. Safety factors of cage at the stage of start-up and stop fall in the ranges of 3.74~13.24 and 6.90~51.58, respectively. The greater the safety factor, the greater the safety characteristic of cage.

*5.3. Influence of Radial Force on Cage Safety Characteristic.* Assume that radial forces are set to 100 N, 500 N, 1000 N, 2000 N, 4000 N, 8000 N, and 10000 N, respectively. Speeds of inner ring are set to 10000 r/min, 20000 r/min, and 30000 r/min, respectively. Acceleration time and deceleration time are set to 0.3 s. Changing trends of maximum von Mises stress with radial force at the connection of crossbeam and side beam are shown in Figure 12.

In Figure 12(a), it is shown that, at the stage of start-up, the maximum von Mises stress at the connection of crossbeam and side beam increases rapidly when radial force $F_r < 4000$ N and then increases slowly when radial force $F_r > 4000$ N. In Figure 12(b), it is shown that, at the stage of stop, the maximum von Mises stress decreases rapidly when radial force $F_r < 4000$ N and then decreases slowly when radial force $F_r > 4000$ N.

Safety factors of cage under different radial forces range from 2.42 to 188.46 at the stage of start-up and 4.67~31.31 at the stage of stop. Possibility of cage's fatigue failure is quite small at the stage of start-up when bearing is working under low radial force, as well as possibility of cage's fatigue at the stage of stop when bearing is working under heavy radial force.

*5.4. Influence of Cage Pocket Circumferential Clearance on Cage Safety Characteristic.* Assuming that radial force $F_r$ is set to 1000 N, cage pocket circumferential clearances are set to 0.24 mm, 0.36 mm, 0.48 mm, 0.6 mm, 0.72 mm, 0.96 mm, and 1.2 mm, respectively. Speeds of inner ring are set to 10000 r/min, 20000 r/min, and 30000 r/min. Acceleration time and deceleration time are set to 0.3 s. Changing trends of maximum von Mises stress with cage pocket circumferential clearance at the connection of crossbeam and side beam are shown in Figure 13.

It can be seen that the maximum von Mises stress at the stage of start-up and stop increases firstly with cage pocket circumferential clearance and then decreases afterwards. Bigger cage pocket circumferential clearance affects cage's strength, as it reduces the width of cage crossbeam. Hence, a smaller cage pocket circumferential clearance is suggested in this study. Referring to [34], the main reasons causing aforementioned phenomenon were as follows: in general, when cage's clearance ratio (clearance ratio = cage pocket circumferential clearance/guide clearance of cage) is small, cage's whirling is relatively stable, but the collision forces between rollers and cage are large. On the contrary, the collision force is relatively small when the clearance ratio is bigger, which can explain why the maximum von Mises stress is relatively smaller when cage pocket circumferential clearance is bigger. Meanwhile, when pocket circumferential clearance is small enough, the roller has not enough distance

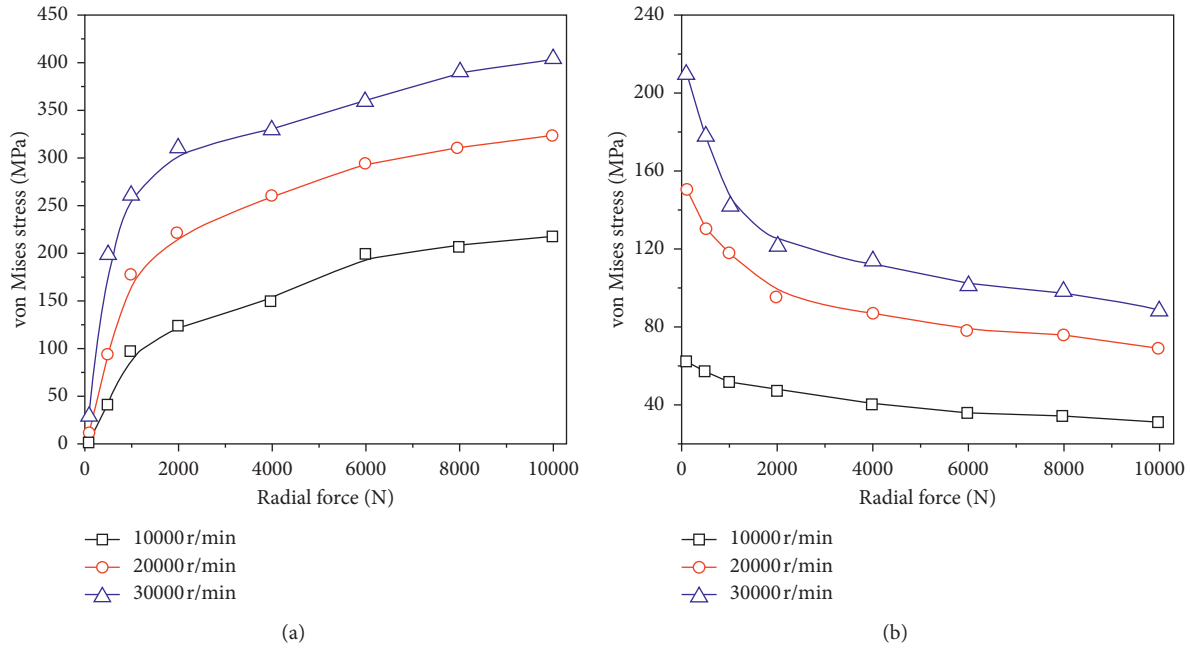


Figure 12: Influence of radial load Fr on cage stress at the stage of start-up and stop. (a) Cage stress at the stage of start-up. (b) Cage stress at the stage of stop.

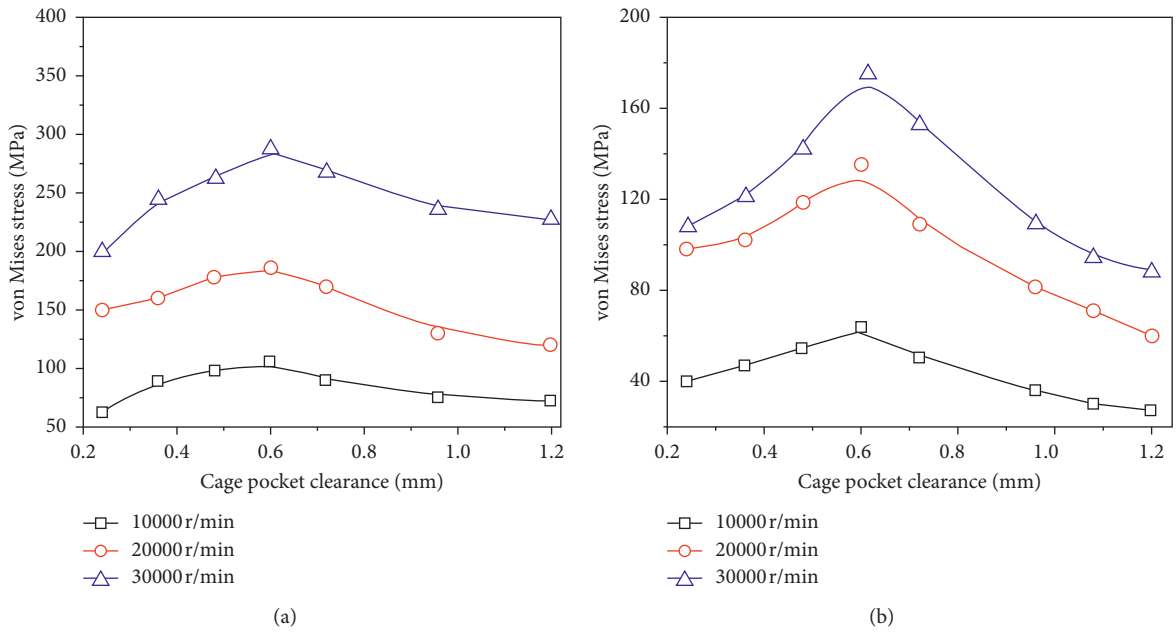


Figure 13: Influence of cage pocket circumferential clearance on cage stress at the stage of start-up and stop. (a) Cage stress at the stage of start-up. (b) Cage stress at the stage of stop.

to accelerate or decelerate in cage pocket, which decreases the speed difference and collision forces between rollers and cage. Therefore, the maximum von Mises stress with the increasing pocket circumferential clearance caused the changing trend in Figure 13 to appear.

Safety factors under different pocket circumferential clearances at the stage of start-up and stop range within 3.40 to 15.81 and 5.47~36.30, respectively. Possibility of cage's fatigue failure at any stage is quite low when cage pocket circumferential clearance is small enough.

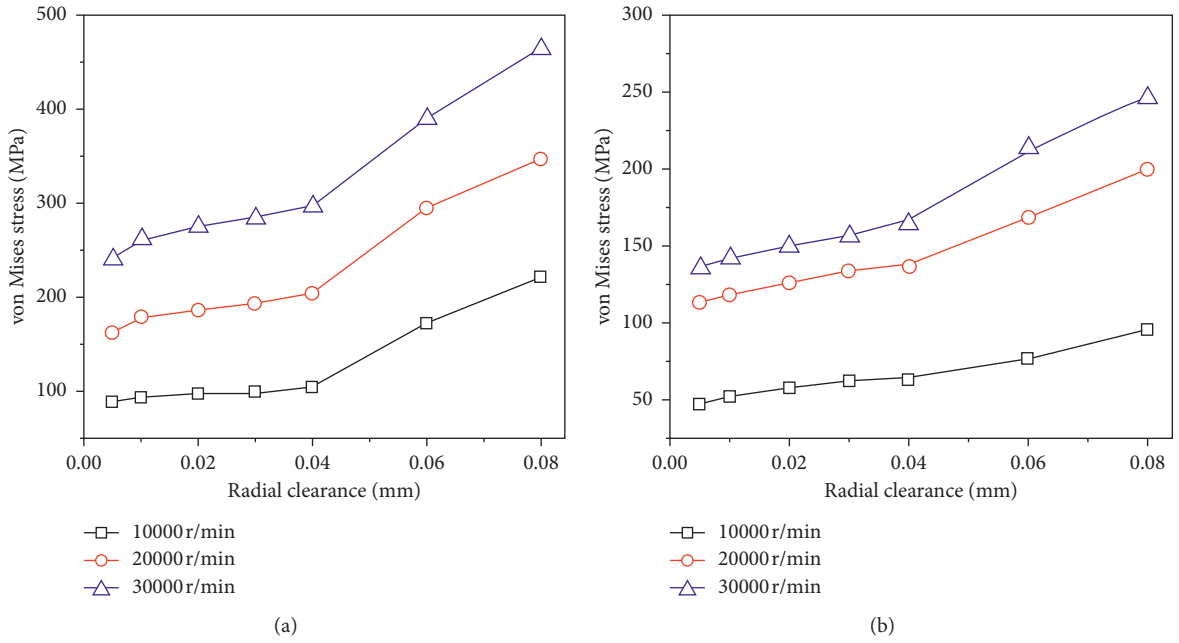


Figure 14: Influence of radial clearance on cage stress at the stage of start-up and stop. (a) Cage stress at the stage of start-up. (b) Cage stress at the stage of stop.

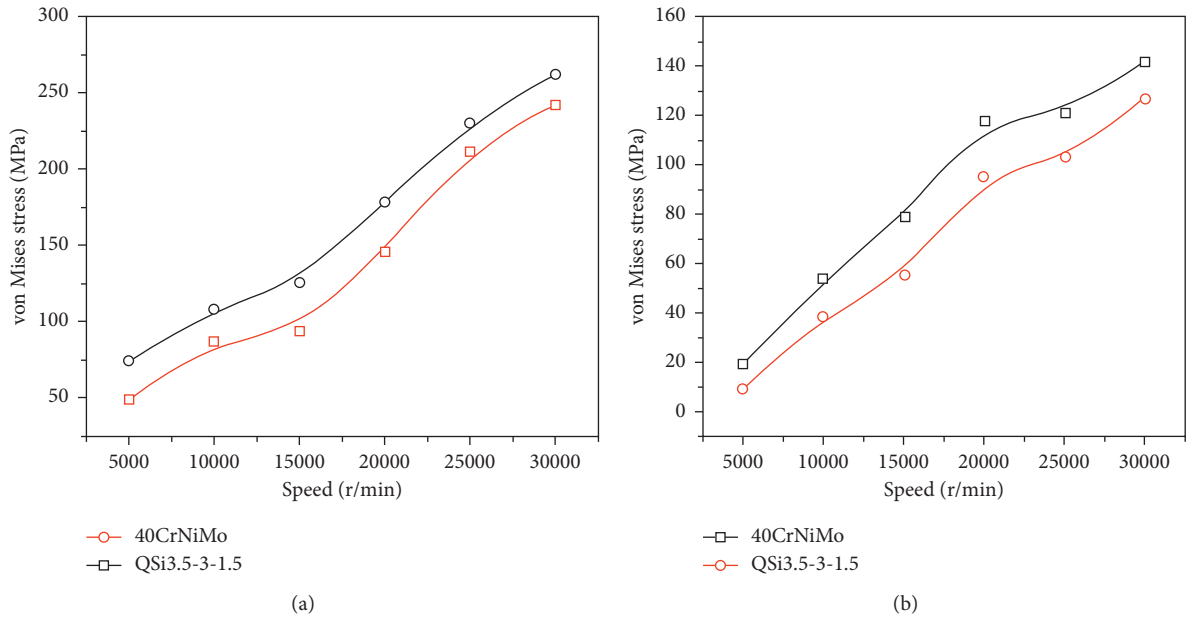


Figure 15: Influence of cage material on cage stress at the stage of start-up and stop. (a) Cage stress at the stage of start-up. (b) Cage stress at the stage of stop.

*5.5. Influence of Radial Clearance on Cage Safety Characteristic.* Assuming that radial force $F_r$ is set to 1000 N, radial clearances are set to 0.005 mm, 0.01 mm, 0.02 mm, 0.03 mm, 0.04 mm, 0.06 mm, and 0.08 mm, respectively. Speeds of inner ring are set to 10000 r/min, 20000 r/min, and 30000 r/min, respectively. Acceleration time and deceleration time are set to 0.3 s. Changing trends of maximum von Mises stress with radial clearance at the connection of crossbeam and side beam are shown in Figure 14.

It can be seen that when radial clearance is smaller than 0.04 mm, the maximum von Mises stress at the stage of start-up and stop increases insignificantly. However, when radial clearance is larger than 0.04 mm, the maximum von Mises stress increases rapidly. It indicates that the larger radial

clearance will cause very intense collision between roller and cage's crossbeam.

Safety factors under different radial clearances at the stage of start-up and stop range from 2.10 to 11.14 and 3.97~20.94, respectively. It can be seen that the safety factors are smaller than what we calculated in Figure 11~13, indicating that bearing radial clearance should be controlled within a certain range firstly, so as to reduce the possibility of cage's fatigue failure.

*5.6. Influence of Cage Material on Cage Safety Characteristic.* Assuming that radial force $F_r$ is set to 1000 N, speeds of inner ring are set to 5000 r/min, 10000 r/min, 15000 r/min, 20000 r/min, 25000 r/min, and 30000 r/min, respectively. Acceleration time and deceleration time are set to 0.3 s. Changing trends of maximum von Mises stress of cage made of different materials (namely, QSi3.5-3-1.5 and 40CrNiMo) are shown in Figure 15. It shows that the maximum von Mises stress of cage made of 40CrNiMo at the stage of start-up and stop is generally larger than cage made of QSi3.5-3-1.5, due to smaller elasticity modulus of QSi3.5-3-1.5.

Safety factors of cage made of 40CrNiMo and cage made of QSi3.5-3-1.5 at the stage of start-up range from 3.74 to 13.24 and 1.86~9.18, respectively. Furthermore, at the stage of stop, safety factors of two materials range from 6.90 to 51.58 and 3.54~44.87, respectively. It can be seen that the maximum von Mises stress of cage made of 40CrNiMo is larger than that of QSi3.5-3-1.5, but safety factor of cage made of 40CrNiMo is actually greater than that of QSi3.5-3-1.5. According to [32], the ultimate tensile strength QSi3.5-3-1.5 is 450 MPa, which explains why safety factor of cage made of 40CrNiMo is bigger than that of QSi3.5-3-1.5. Therefore, in this paper, it is suggested to use cage made of 40CrNiMo at the stage of rapid start-up and stop.

## 6. Conclusions

(1) The maximum von Mises stress at the connection of crossbeam and side beam at the stage of start-up emerges in the middle of connection. However, at the stage of stop, due to the effect of cage's high speed, the maximum von Mises stress at the connection of crossbeam and side beam is close to cage's external surface.

(2) At the stage of start-up and stop, the maximum von Mises stress increases with the acceleration of inner ring, and the safety factor at the stage of start-up is generally smaller than that at the stage of stop, indicating that cage at the stage of start-up is much easier to suffer fatigue failure compared to that at the stage of stop.

(3) At the stage of start-up, safety factor at the connection of crossbeam and side beam increases with radial force. However, for the safety factor at the stage of stop, changing trend is opposite to that at the stage of start-up. Therefore, a small radial force should be applied at the stage of start-up and a large radial force should be applied at the stage of stop.

(4) The maximum von Mises stress at the stage of start-up and stop increases firstly with cage pocket circumferential clearance and then decreases afterwards. The safety factor displays an opposite trend. Considering that a big cage pocket circumferential clearance reduces cage's strength, a small cage pocket circumferential clearance is suggested.

(5) At the stage of start-up and stop, a large radial clearance leads to large von Mises stress and small safety factor at the connection of crossbeam and side beam, so it suggests that radial clearance must be controlled within a certain range firstly, and it should be smaller than 0.04 mm as suggested in this paper.

(6) Cage's material with smaller elasticity modulus (QSi3.5-3-1.5) is beneficial to reduce the maximum von Mises stress; nevertheless, 40CrNiMo is still recommended due to its greater ultimate tensile strength as compared to that of QSi3.5-3-1.5.

## Data Availability

The data used to support the findings of this study are available from the corresponding author upon request.

## Conflicts of Interest

The authors declare that there are no conflicts of interest regarding the publication of this paper.

## Acknowledgments

This research was financially supported by Youth Program of National Natural Science Foundation of China (51905152), Science and Technology Program of Shenzhen (JCYJ20170818114408837), and China Postdoctoral Science Foundation (2020M671276).

## References

[1] P. K. Gupta, "Dynamics of rolling-element bearings-part I: cylindrical roller bearing analysis," *Journal of Lubrication Technology*, vol. 101, no. 3, pp. 293–302, 1979.

[2] P. K. Gupta, "On the frictional instabilities in a cylindrical roller bearing," *Tribology Transactions*, vol. 33, no. 3, pp. 395–401, 1990.

[3] P. K. Gupta, "Modeling of instabilities induced by cage clearances in cylindrical roller bearings," *Tribology Transactions*, vol. 34, no. 1, pp. 1–8, 1991.

[4] N. Ghaisas, C. R. Wassgren, and F. Sadeghi, "Cage instabilities in cylindrical roller bearings," *Journal of Tribology*, vol. 126, no. 4, pp. 681–689, 2004.

[5] T. Jafar and M. M. Khonsari, "On the influence of traction coefficient on the cage angular velocity in roller bearings," *Tribology Transactions*, vol. 57, pp. 793–805, 2014.

[6] L. Cui, L. Q. Wang, D. Z. Zheng et al., "Analysis on dynamic characteristics of aero-engine high-speed roller bearing," *ActaAeronautica et Astronauticasinica*, vol. 29, no. 2, pp. 492–498, 2008.

[7] H. Yang, "Flexible Dynamic simulation on cage of aero engine high speed cylindrical roller bearings," *Bearing*, vol. 2, pp. 7–11, 2011.

[8] X. H. Liu, S. E. Deng, and H. F. Teng, "Kinematics analysis of cages in high-speed cylindrical roller bearings," *Aeroengine*, vol. 39, no. 2, pp. 31–38, 2013.

[9] S. E. Deng, J. F. Gu, Y. C. Cui et al., "Analysis on dynamic characteristics of cage in high-speed cylindrical roller bearing," *Journal of Aerospace Power*, vol. 29, no. 1, pp. 492–498, 2014.

[10] L. Chen, X. Xia, H. Zheng, and M. Qiu, "Chaotic dynamics of cage behavior in a high-speed cylindrical roller bearing," *Shock and Vibration*, vol. 2016, pp. 1–12, 2016.

[11] N. Fang, D. Pugh, and R. Themudo, "On the stress concentration factors of rolling element bearing cages," *Tribology Transactions*, vol. 50, no. 4, pp. 445–452, 2007.

[12] A. Dib and A. Haiahem, "FEM analysis of cage stress distribution: Part1: cylindrical roller bearing," *Journal of Engineering & Applied Sciences*, vol. 2, no. 1, pp. 180–182, 2012.

[13] H. S. Yang, G. D. Chen, S. E. Deng et al., "Rigid-flexible coupled dynamic simulation of aeroengine main-shaft high speed cylindrical roller bearing," *Advanced Computer Theory and Engineering* in *Proceedings of the 2010 3rd International Conference*, no. 4, pp. 31–35, August 2010, Chengdu, China.

[14] M. Li, "Slip characteristics of high-speed cylindrical roller bearing at stop stage," *Journal of Henan University of Science and Technology*, vol. 36, no. 6, pp. 14–19, 2015.

[15] Y. C. Jia and S. E. Deng, "Analysis of slippage characteristic of roller in cylindrical roller bearing during the start up," *Journal of Mechanical Transmission*, vol. 39, no. 12, pp. 133–137, 2015.

[16] H. F. Ding, M. Jing, and F. Wang, "Skidding analysis of high speed cylindrical roller bearing considering acceleration of bearing," *Machinery Design and Manufacture*, vol. 2, pp. 64–67, 2016.

[17] Y. C. Cui, S. E. Deng, and W. H. Zhang, "The impact of roller dynamic unbalance of high-speed cylindrical roller bearing on the cage nonlinear dynamic characteristics," *Mechanism & Machine Theory*, vol. 118, pp. 65–83, 2017.

[18] Y. Cui, S. Deng, R. Niu, and G. Chen, "Vibration effect analysis of roller dynamic unbalance on the cage of high-speed cylindrical roller bearing," *Journal of Sound and Vibration*, vol. 434, pp. 314–335, 2018.

[19] Y. Cui, Y. S. Deng, and G. Chen, "Effect of roller dynamic unbalance on cage stress of high-speed cylindrical roller bearing," *Industrial Lubrication and Tribology*, vol. 70, no. 9, pp. 1580–1589, 2018.

[20] Y. Cui, S. Deng, H. Yang, and W. Zhang, "Effect of cage dynamic unbalance on the cage's dynamic characteristics in high-speed cylindrical roller bearings," *Industrial Lubrication and Tribology*, vol. 71, no. 10, pp. 1125–1135, 2019.

[21] Q. Niu, X. Li, and F. Chu, "Skidding behavior of cylindrical roller bearings under time-variable load conditions," *International Journal of Mechanical Sciences*, vol. 135, pp. 203–214, 2017.

[22] X. Sun, S. E. Deng, and G. D. Chen, "Vibration characteristics analysis of high-speed cylindrical roller bearings with elastic supports," *Journal of Vibration and Shock*, vol. 36, no. 18, pp. 20–28, 2017.

[23] S. Deng, Y. Lu, W. Zhang, X. Sun, and Z. Lu, "Cage slip characteristics of a cylindrical roller bearing with a trilobe-raceway," *Chinese Journal of Aeronautics*, vol. 31, no. 2, pp. 351–362, 2018.

[24] W. Zhang, S. Deng, G. Chen, and Y. Cui, "Impact of lubricant traction coefficient on cage's dynamic characteristics in high-speed angular contact ball bearing," *Chinese Journal of Aeronautics*, vol. 30, no. 2, pp. 827–835, 2017.

[25] T. Sakaguchi and K. Ueno, "Dynamic analysis of cage behavior in a cylindrical roller bearing," *NTN Technical Review*, vol. 71, pp. 8–17, 2004.

[26] W. H. Zhang, S. E. Deng, and G. D. Chen, "Influence of lubricant traction coefficient on cage's nonlinear dynamic behavior in high-speed cylindrical roller bearing," *Journal of Tribology*, vol. 139, no. 6, Article ID 061502, 2017.

[27] Z. Guo, R. Xu, and P. Xue, "Study on preparation of ultra-high-molecular-weight polyethylene pipe of good thermal-mechanical properties modified with organo-montmorillonite by screw extrusion," *Materials*, vol. 13, no. 15, p. 3342, 2020.

[28] H. M. Hilber, T. J. R. Hughes, and R. L. Taylor, "Improved numerical dissipation for time integration algorithms in structure dynamics," *Earthquake Engineering & Structural Dynamics*, vol. 5, no. 3, pp. 283–292, 1977.

[29] A. Basumallik, S. J. Min, and R. Eigenmann, "Programming distributed memory systems using OpenMP," in *Proceedings of the 2007 IEEE International Parallel and Distributed Processing Symposium*, Rome, Italy, March 2007.

[30] B. T. Mattson, "Introduction to OpenMP–tutorial," in *Proceedings of the ACM/IEEE Sc2006 Conference on High Performance Networking and Computing*, Universität Stuttgart, Stuttgart, Germany, 2010.

[31] L. M. Surhone, M. T. Timpledon, and S. F. Marseken, *Von Mises Yield Criterion*, Betascript Publishing, Beau Bassin, Mauritius, 2010.

[32] R. C. Juvinall, *Engineering Considerations of Stress, Strain, and Strength*, McGraw-Hill, New York, NY, USA, 1967.

[33] A. B. Makar, K. E McMartin, M Palese, and T. R Tephly, "Formate assay in body fluids: application in methanol poisoning," *Biochemical Medicine*, vol. 13, no. 2, pp. 117–126, 1975.

[34] T. Yoshio, "The dynamic whirle of angular contact ball bearing cages," *Bearing*, no. 3, pp. 14–21, 1995.